Available online at www.sciencedirect.com
SCIENCE DIRECT®
Journal of Sound and Vibration 278 (2004) 749–772
JOURNAL OF SOUND AND VIBRATION
www.elsevier.com/locate/jsvi

Modelling turbulence-induced vibration of pipes with a spectral finite element method

F. Birgersson[a], S. Finnveden[a,*], G. Robert[b]

[a] *MWL, Aeronautical and Vehicle Engineering, KTH, SE-100 44 Stockholm, Sweden*
[b] *Labarotoire de Méchanique des Fluides et d'Acoustique, UMR CNRS 5509, École Centrale de Lyon, BP 163, 69131 Ecully Cedex, France*

Received 16 May 2003; accepted 15 October 2003

Abstract

The vibration of pipes is studied here using the Arnold–Warburton theory for thin shells and a simplified theory valid in a lower frequency regime. The vibrational response is described numerically with the spectral finite element method (SFEM), which uses the exact solutions of the equations of motion as basis functions. For turbulence excitation, the set of basis functions was extended to include particular solutions, which model a spatially distributed excitation. An efficient numerical solution to homogeneous random excitation is presented and the results compare favourably with wind tunnel measurements.

1. Introduction

The study of turbulent boundary layer (TBL)-induced vibration of structures is a problem that involves the coupling of structural and fluid vibration. It is of great practical importance to a number of fields, especially so whenever this flow-induced vibration leads to structural fatigue or excessive noise. Many studies related to the problem in the literature consider only thin elastic plates excited by turbulent flow, although some recent studies on pipe structures are available, e.g., Refs. [1,2]. Both these studies use a normal mode approach.

The spectral finite element method (SFEM) is a direct finite element method for analyzing vibrations in built-up structures [3–5]. The frequency-dependent formulation remedies some of the restrictions of the standard FEM. Thus, it is inherently simple to handle frequency-dependent material characteristics and boundary conditions. Most importantly, dissipative wave motion within large elements can be studied with computational efficiency.

*Corresponding author.
E-mail address: svantef@kth.se (S. Finnveden).

0022-460X/$ - see front matter
doi:10.1016/j.jsv.2003.10.024

The response to distributed stochastic excitation, such as TBL excitation, is most often found by a double integral over the structure, where the integrand is given by the cross-spectral density of the forcing and the structure's Green function, see Ref. [6]. This may lead to impossibly large numerical computations. In an alternative formulation, Newland and also Lin [7] Fourier transforms the cross-spectral density and derives the response as a single integral over the wavenumber domain. In this formulation, the integrand is given by the excitation's wavevector-frequency spectrum and the structure's sensitivity function, given as the response to a travelling pressure wave. This approach is applied here to the case of TBL excitation and provides for an efficient numerical solution to this type of problems. This wavevector-frequency approach [5,8] has two main advantages. First, it reduces the computational effort and second it allows for a physical interpretation of the problem. The vibro-acoustic response can be interpreted as the result of passing the excitation spectrum through a filter, characterized by the sensitivity function, which only depends on the geometrical and mechanical properties of the structure.

Langley presented a dynamic stiffness method formulation for the calculation of the sensitivity function for a simply supported plate structure [9]. This formulation was investigated in detail in Ref. [10] for beams and simply supported plate structures, demonstrating the feasibility of the approach, but also deriving similar sensitivity functions for the SFEM. These functions were then successfully used, when predicting the TBL-induced vibration of simply supported plates in Ref. [5].

The measurements of the TBL-induced vibration of a thin-walled cylindrical shell, which are used to assess the developed theory, were made in a wind tunnel specifically designed to minimize acoustic contamination. Flow velocities of up to 120 m/s could be obtained in the test section. The experimental facility and the measured characteristics of the wall pressure field have been presented in detail in Ref. [11] and more briefly in Ref. [1].

The measured power spectral density, correlation lengths and convection velocity were included in a semi-empirical model developed by Corcos [12]. This model was tentatively used in this study for the numerical predictions. It is completely valid only at or near the convective wavenumber, and therefore various other models have been developed in the wavevector-frequency domain to increase the range of validity, see for example Refs. [13,14]. These models and similar models can be included in the computational scheme presented here.

The outline of this paper is as follows. First general equations of motion for thin-walled pipes are discussed. No fluid–structure interaction was considered here due to the relatively weak coupling between structure and air, but it is recommended that for a pipe filled with a heavier fluid at least a first order approximation be made to the equations of motion, e.g., as suggested in reference [15, Eq. (28)]. From the Arnold–Warburton theory a simplified theory is derived, similar to Ref. [15], which is valid for long axial wavelengths and in-extensional circumferential motion. Ref. [15] shows that wavenumbers in fluid-filled pipes can be predicted with this simplified theory. Here it is also shown how the forced response can be calculated. In Section 3, the response of a pipe to a travelling pressure wave is calculated, i.e., the sensitivity function. Given this sensitivity function, Section 4 derives a method to predict the response of the structure to TBL excitation. In Section 5, the results from the simplified cylinder theory are first compared to those from the full Arnold–Warburton theory and then used to predict the structural response to TBL flow. The results compare favourably with the measurements.

2. General and simplified equations of motion for thin-walled cylindrical pipes

Using variational principles, both general and simplified equations of motion for thin-walled pipes are derived in this section. To predict random vibration a formulation in the frequency domain is used. The work done by a travelling pressure wave is also considered, as the response to such a wave will be of interest in later sections.

2.1. Hamilton's variational principle

Consider the thin-walled cylinder in Fig. 1, where R is the radius, l_x is half the length, and h is the wall-thickness. u, v and w are the displacements on the cross-sectional mid-plane in the x, ϕ and z directions, respectively. To derive the equations of motion of the cylinder Hamilton's principle will be used. It states that the variation of the time integral between given time limits of the difference between the kinetic energy e_{kin} and potential energy e_{pot} must vanish, i.e.,

$$\delta \int_{t_1}^{t_2} (e_{pot} - e_{kin})\, \mathrm{d}t = 0. \tag{1}$$

The first step is to find expressions for these different energies.

The total strain energy of a circular cylindrical shell is given by Leissa [16, Eq. (2.10)]

$$e_{pot} = \frac{Eh}{2(1-\nu^2)} \int_0^{2\pi} \int_{-l_x/R}^{l_x/R} (I_{D-M}(u,v,w) + \beta I_{MOD}(u,v,w))\, \mathrm{d}s\, \mathrm{d}\varphi, \tag{2}$$

where

$$\beta = h^2/12R^2 \quad \text{and} \quad s = x/R. \tag{3}$$

E denotes Young's modulus and ν is the Poisson ratio. I_{D-M} is the integrand of the strain energy of the shell according to the Donnell–Mushtari theory and is given in Ref. [16, Eq. (2.11)]. I_{MOD} is a "modifying integrand" which differs depending on shell theory. In this study the

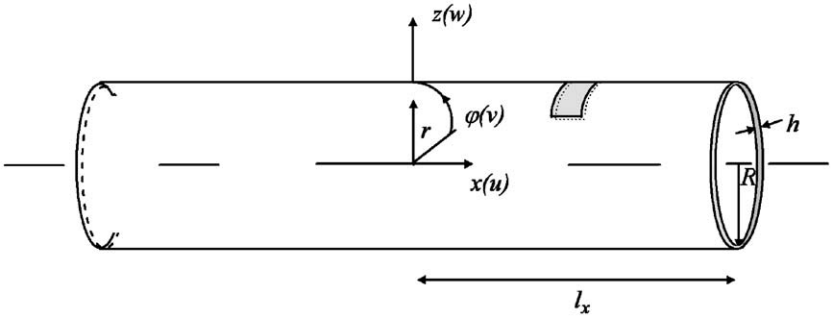

Fig. 1. The cylinder co-ordinate system with displacements.

Arnold–Warburton (also Goldenveizer–Novozhilov and modified Love–Timoshenko) theory was chosen, in which case I_{MOD} is given in Ref. [16, Eq. (2.12a)].

The kinetic energy of the cylinder is [16, Eq. (2.14)]

$$e_{kin} = \tfrac{1}{2}\rho h R^2 \int_0^{2\pi} \int_{-l_x/R}^{+l_x/R} \left(\left(\frac{\partial u}{\partial t}\right)^2 + \left(\frac{\partial v}{\partial t}\right)^2 + \left(\frac{\partial w}{\partial t}\right)^2 \right) \mathrm{d}s\, \mathrm{d}\varphi, \tag{4}$$

where ρ is density of the shell.

With the calculus of variations, the equations of motion for the cylindrical pipe can be found, see Ref. [16, Eqs. (2.3)–(2.9)].

2.2. Variational principle for harmonic vibration of non-conservative systems

For random response it is convenient to study motion in the frequency domain. For free harmonic motion, the displacement functions are of the form $\mathrm{e}^{\mathrm{i}\omega t}$. These functions are substituted into Eq. (1). One then lets $t_{1,2} \to \pm\infty$ and apply Parseval's identity. The governing equations are linear and thus the different frequency components in the resulting integral do not couple with each other. Upon this analysis follows a bi-linear functional of the displacements at a given frequency and their complex conjugates, which is stationary for the true motion.

With dissipative losses though, Hamilton's principle is not valid. However, these losses may be attributed by employing a variational principle similar to that of Hamilton, see Refs. [3,17]. Thus, the bi-linear forms in the displacements and its complex conjugates are replaced with bi-linear forms in the displacements and in the complex conjugates of the displacements in an adjoint negatively damped system. This is conceptually more complex, but the approach requires no extra calculation effort. The function considered is thus given by

$$\begin{aligned} L = \int_0^{2\pi} \int_{-l_x/R}^{+l_x/R} \Big\{ & \frac{Eh}{(1-\nu^2)} (I_{D\text{–}M}(U, V, W, U^a, V^a, W^a) \\ & + \beta I_{MOD}(U, V, W, U^a, V^a, W^a)) - \rho h R^2 \omega^2 (U^a U + V^a V + W^a W) \Big\} \mathrm{d}s\, \mathrm{d}\varphi, \end{aligned} \tag{5}$$

where superscript a denotes the complex conjugate in an adjoint negatively damped system. The terms $I_{D\text{–}M}$ and I_{MOD} are similar to the ones by Leissa [16, Eqs. (2.11) and (2.12a)], except that these terms are functions of the displacements and the displacement functions in an adjoint system. They are listed in Appendix A. Integral (5) will be referred to as the Lagrangian.

The virtual work of a distributed pressure acting on the pipe is given by, cf. Refs. [3,10],

$$L_p = \int_0^{2\pi} \int_{-l_x}^{l_x} (p^* W + p W^a)\, \mathrm{d}x\ R\, \mathrm{d}\varphi, \tag{6}$$

where * denotes complex conjugate.

2.3. Arnold–Warburton theory

The motion of the cylinder is now investigated using a Fourier decomposition of the circumferential dependence of the displacements, similar to Ref. [16, Eq. (2.20)],

$$\begin{aligned} U(x,\varphi) &= U_n(x)\cos(n\varphi),\\ V(x,\varphi) &= V_n(x)\sin(n\varphi),\\ W(x,\varphi) &= W_n(x)\cos(n\varphi), \end{aligned} \tag{7}$$

where n is an integer greater or equal to zero for the closed shell. The mode $n=0$ will not be investigated further in this paper, because below the ring frequency, ($f_{ring}=\sqrt{E/\rho(1-\nu^2)}/2\pi R$), this mode does not contribute much to the vibration. Displacements (7) are inserted into Lagrangian (5) and the integral over ϕ is evaluated. Appendix A.1 lists the resulting Lagrangian L_n with its numerous terms for all circumferential modes n.

2.4. Simplified theory

At this stage it was also of interest to derive a simplified Lagrangian to ease the understanding of the underlying parameters, when modelling pipe vibrations below the ring frequency. Here the same assumptions as in Ref. [15] are made:

The wavelength λ is large compared to the cylinder radius, i.e.,

$$\lambda > 2\pi R. \tag{8}$$

The circumferential in-plane motion is in-extensional and thus the in-plane strain of the cylinder for mode n is given by

$$\varepsilon_{n\varphi} = (nV_n(x) + W_n(x))/R = 0, \quad n \geqslant 1. \tag{9}$$

Given expression (9), the number of terms in the Lagrangian L_n are greatly reduced. The strain energy caused by the flexural motion of the shell wall now contains terms that depend only on the radial motion. Given assumption (8), the potential energy from axial bending is less than those from twist and circumferential bending and may be neglected for low frequencies. Furthermore, numerical experiments [15] revealed, that changing the axial stiffness from $EA/(1-\nu^2)$ to EA, made the predicted wavenumbers agree better with the more exact Arnold–Warburton theory. The terms in the resulting simplified Lagrangian are listed in Appendix A.2.

Now, consider a distributed excitation in the form of a travelling pressure wave in the x and ϕ directions

$$p(x,\varphi,t) = p_0 \mathrm{e}^{-\mathrm{i}\alpha_m x}\cos(n\varphi)\mathrm{e}^{\mathrm{i}\omega t}. \tag{10}$$

This pressure excites only mode n and the virtual work (6) is

$$\int_{-l_x}^{l_x} (P_n \mathrm{e}^{-\mathrm{i}\alpha_m x})^* W_n + (P_n \mathrm{e}^{-\mathrm{i}\alpha_m x}) W_n^a \,\mathrm{d}x, \tag{11}$$

where

$$P_n = \int_0^{2\pi} p_0 \cos^2(n\varphi) R \,\mathrm{d}\varphi = p_0 \pi R. \tag{12}$$

This virtual work results from external forces and is thus subtracted from Lagrangian (5). Collecting terms in Appendix A.2 and applying the modifications discussed above, the following simplified Lagrangian is derived

$$L_n = \int_{-l_x}^{l_x} \left\{ EI_n \frac{\mathrm{d}\theta_n^a}{\mathrm{d}x}\frac{\mathrm{d}\theta_n}{\mathrm{d}x} + GAK_n\left(\theta_n^a + \frac{\mathrm{d}W_n^a}{\mathrm{d}x}\right)\left(\theta_n + \frac{\mathrm{d}W_n}{\mathrm{d}x}\right) + GAK_nN_n\frac{\mathrm{d}W_n^a}{\mathrm{d}x}\frac{\mathrm{d}W_n}{\mathrm{d}x} + (K_w - \omega^2 M_e)W_n^a W_n - \rho\omega^2 I_n\theta_n^a\theta_n - (P_n\mathrm{e}^{-\mathrm{i}\alpha_m x})^* W_n - (P_n\mathrm{e}^{-\mathrm{i}\alpha_m x})W_n^a \right\} \mathrm{d}x, \tag{13}$$

where the damping is described with a complex Young's modulus $E(1+\mathrm{i}\eta)$ and

$$\theta_n = n^2 U_n / R. \tag{14}$$

The coefficients in Eq. (13) are

$$M_e = \frac{\rho A}{2}(1 + 1/n^2), \quad I_n = \frac{\pi h R^3}{n^4}, \quad K_n = \frac{1}{2n^2}, \quad A = 2\pi hR,$$
$$K_w = \frac{EA(n^2-1)^2}{(1-\nu^2)2R^2}\beta, \quad N_n = 4n^2(n - 1/n)^2\beta, \quad G = \frac{E}{2(1+\nu)}. \tag{15}$$

With the calculus of variation, the equations of motion corresponding to the simplified Lagrangian are found to be

$$EI_n\frac{\mathrm{d}^2\theta_n}{\mathrm{d}x^2} - GAK_n\left(\theta_n + \frac{\mathrm{d}W_n}{\mathrm{d}x}\right) + \rho\omega^2 I_n\theta_n = 0, \tag{16}$$

$$GAK_n\left(\frac{\mathrm{d}}{\mathrm{d}x}\left(\theta_n + \frac{\mathrm{d}W_n}{\mathrm{d}x}\right) + N_n\frac{\mathrm{d}^2 W_n}{\mathrm{d}x^2}\right) - (K_w - \omega^2 M_e)W_n = P_n\mathrm{e}^{-\mathrm{i}\alpha_m x}. \tag{17}$$

Eqs. (13), (16) and (17) will be used in the following section for the spectral FE formulation.

3. Spectral FE formulation for distributed sources

In this section the sensitivity function is derived. It is the structural response of the pipe to a travelling pressure wave. The procedure is only shown here for the simplified cylinder theory, derived previously, but the same method applies also to the more general Arnold–Warburton theory. First the exact displacement functions are found to the governing equations of motion. These are expressed as functions of the nodal displacements and substituted into the Lagrangian. By requiring that the first variation of this Lagrangian with respect to the nodal displacements is zero, a system of equations for the nodal displacements is derived. Given these displacements, the response of the pipe is described.

3.1. Exact displacement functions

With no pressure excitation, the system of Eqs. (16) and (17) is homogeneous and has constant coefficients. Its solutions are then of the form $e^{k_{ni}x}$. The constants k_{ni} are here denoted wavenumbers and may be real, imaginary or complex, describing decaying nearfield solutions, propagating or decaying oscillating waves, respectively. The solutions are given by a linear eigenvalue problem, detailed in Appendix B. To gain numerical stability for long elements, these solutions are scaled as in Ref. [4],

$$\begin{pmatrix} W_n(x) \\ \theta_n(x) \end{pmatrix}_{\mathbf{h}} = (\mathbf{\Psi}\,\mathrm{diag}(e^{\mathbf{K}x-\mathbf{K}_p l_x}))\mathbf{C}_n, \tag{18}$$

where

$$\begin{aligned} &\mathbf{K} = (k_{n1} \quad k_{n2} \quad k_{n3} \quad k_{n4}), \quad \mathbf{C}_n = (C_{n1} \quad C_{n2} \quad C_{n3} \quad C_{n4})^{\mathrm{T}}, \\ &\mathbf{\Psi} = \begin{pmatrix} \mathbf{B}_W \\ \mathbf{B}_\theta \end{pmatrix}, \quad (\mathbf{K}_p)_i = \begin{cases} -\mathbf{K}_i, & \mathrm{Re}(\mathbf{K}_i) \leqslant 0, \\ \mathbf{K}_i, & \text{else.} \end{cases} \end{aligned} \tag{19}$$

The vector $\mathbf{K}$ contains the four wavenumbers k_{ni}, whereas $\mathbf{C}_n$ contains the wave amplitudes. The function 'diag' produces a diagonal matrix from a vector, similar to MATLAB. $\mathbf{B}_W$ and $\mathbf{B}_\theta$ are row vectors given by the eigenvectors corresponding to the eigenvalues k_{ni}, see the appendix. Eq. (18) gives the exact solutions to the homogeneous equations of motion (16) and (17).

The particular solution to Eqs. (16) and (17) is of the form

$$\begin{pmatrix} W_n(x) \\ \theta_n(x) \end{pmatrix}_{\mathbf{p}} = \mathbf{C}_{np} e^{-i\alpha_m x}, \tag{20}$$

where $\mathbf{C}_{np} = (c_{nW} \;\; c_{n\theta})^{\mathrm{T}}$. Inserting this solution into the equations of motion produces

$$EI_n(-\alpha_m^2)c_{n\theta} - GAK_n(c_{n\theta} - i\alpha_m c_{nW}) + \rho\omega^2 I_n c_{n\theta} = 0, \tag{21}$$

$$GAK_n(-i\alpha_m c_{n\theta} - \alpha_m^2 c_{nW} - N_n\alpha_m^2 c_{nW}) - (K_w - \omega^2 M_e)c_{nW} = P_n. \tag{22}$$

This system is easily solved for the two unknown parameters c_{nW} and $c_{n\theta}$, and thus the particular solution is found.

The exact displacement function is given by both homogenous (18) and the particular solution (20) as

$$\mathbf{V}_n(x) = (\mathbf{\Psi}\,\mathrm{diag}(e^{\mathbf{K}x-\mathbf{K}_\mathbf{p} l_x}))\mathbf{C}_n + \mathbf{C}_{np} e^{-i\alpha_m x}, \tag{23}$$

where

$$\mathbf{V}_n(x) = (W_n(x) \quad \theta_n(x))^{\mathrm{T}}. \tag{24}$$

The unknown wave amplitudes $(\mathbf{C}_n)_i$ can be related to the nodal displacements $\mathbf{W}_n = (w_1 \;\; \theta_1 \;\; w_2 \;\; \theta_2)^{\mathrm{T}}$ at the ends of the cylinder with

$$\begin{pmatrix} \mathbf{V}_n(-l_x) \\ \mathbf{V}_n(+l_x) \end{pmatrix} = \mathbf{W}_n. \tag{25}$$

This nodal vector $\mathbf{W}_n$ now contains the degrees of freedom in the element formulation. Solving Eq. (25) for $\mathbf{C}_n$ gives that

$$\mathbf{C}_n = \mathbf{A}(\mathbf{W}_n - \mathbf{W}_{nc}), \tag{26}$$

where

$$\mathbf{A} = \begin{pmatrix} \mathbf{\Psi}\,\mathrm{diag}(\mathrm{e}^{\mathbf{K}(-l_x)-\mathbf{K}_\mathbf{p}l_x}) \\ \mathbf{\Psi}\,\mathrm{diag}(\mathrm{e}^{\mathbf{K}(+l_x)-\mathbf{K}_\mathbf{p}l_x}) \end{pmatrix}^{-1}, \quad \mathbf{W}_{nc} = \begin{pmatrix} \mathbf{C}_{np}\mathrm{e}^{-\mathrm{i}\alpha_m(-l_x)} \\ \mathbf{C}_{np}\mathrm{e}^{-\mathrm{i}\alpha_m(+l_x)} \end{pmatrix}. \tag{27}$$

Finally, this solution for $\mathbf{C}_n$ is inserted into Eq. (23), which gives that

$$\begin{aligned} \mathbf{V}_n(x) &= (\mathbf{\Psi}\,\mathrm{diag}(\mathrm{e}^{\mathbf{K}x-\mathbf{K}_p l_x}))\mathbf{A}(\mathbf{W}_n - \mathbf{W}_{nc}) + \mathbf{C}_{np}\mathrm{e}^{-\mathrm{i}\alpha_m x}, \\ &= (\mathbf{\Psi}\,\mathrm{diag}(\mathrm{e}^{\mathbf{K}x-\mathbf{K}_p l_x}))\mathbf{A}\mathbf{W}_n + \mathbf{B}\,\mathrm{diag}(\mathrm{e}^{\boldsymbol{\alpha}_\mathbf{K}x-\boldsymbol{\alpha}_{\mathbf{K}p}l_x})\mathbf{W}_{np}, \end{aligned} \tag{28}$$

where

$$\begin{aligned} \mathbf{W}_{np} &= (-(\mathbf{A}\mathbf{W}_{nc})^{\mathrm{T}} \quad 1)^{\mathrm{T}}, \quad \mathbf{B} = (\mathbf{\Psi} \quad \mathbf{C}_{np}), \\ \boldsymbol{\alpha}_\mathbf{K} &= (\mathbf{K} \quad -\mathrm{i}\alpha_m), \quad \boldsymbol{\alpha}_{\mathbf{K}p} = (\mathbf{K}_p \quad 0). \end{aligned} \tag{29}$$

Eq. (28) gives the exact solutions to the differential equations (16) and (17), for all travelling pressure waves described by Eq. (10). These exact solutions are taken as basis functions in a frequency-dependent spectral finite element formulation for the cylindrical pipe, which is described in what follows.

3.2. Spectral FE formulation

The displacement functions are expressed by Eq. (28). Similarly, the displacement functions for the adjoint system are given as

$$\mathbf{V}_n^a(x) = (\mathbf{\Psi}\,\mathrm{diag}(\mathrm{e}^{\mathbf{K}x-\mathbf{K}_\mathbf{p}l_x}))\mathbf{A}\mathbf{W}_n^a + \mathbf{B}\,\mathrm{diag}(\mathrm{e}^{\boldsymbol{\alpha}_\mathbf{K}^a x-\boldsymbol{\alpha}_{\mathbf{K}p}l_x})\mathbf{W}_{np}^a, \tag{30}$$

where $\mathbf{W}_{np}^a$ and $\boldsymbol{\alpha}_\mathbf{K}^a$ are found in the same way as described in Section 3.1. Lagrangian (13) is evaluated by substituting the components of $\mathbf{V}_n$ and $\mathbf{V}_n^a$ into it. The integrals and derivatives, involving exponential functions, are then evaluated exactly, without any need for numerical quadrature. By requiring that the first variation of this Lagrangian with respect to the nodal displacement $\mathbf{W}_n^a$ is zero, a system of equations for the nodal displacement $\mathbf{W}_n$ is found,

$$\mathbb{D}_n\mathbf{W}_n = \mathbf{F}_n, \tag{31}$$

where the dynamic stiffness matrix $\mathbb{D}_n$ and the nodal force vector $\mathbf{F}_n$ are detailed in Appendix C together with a derivation of the quantities. The dynamic stiffness matrix does not depend on the excitation and for a general source, described by a superposition of pressure wave excitations, it is therefore only the nodal force vector that needs to be recalculated. Eq. (31) describes one spectral finite element. It has compact support and is formulated in terms of nodal displacements at the ends. It can therefore be assembled using standard methods, e.g., Ref. [18], into a global dynamic stiffness matrix.

For a pipe structure with clamped boundary conditions there is no nodal displacement at the ends. By assembling two elements, however, the nodal displacement at the joint of the elements

can be varied. Similar to the FEM, the phase of the pressure in a global co-ordinate system now has to be transformed to the local co-ordinate system of the two elements.

3.3. Sensitivity function

Solving Eq. (31) gives the nodal displacements $\mathbf{W}_n$ of the structure, when excited by a pressure wave $p_0 e^{-i\alpha_m x} \cos(n\varphi)$. Given $\mathbf{W}_n$, the modal response of the structure $W_n(x)$ is given by Eq. (28). For future reference, the modal response to a pressure wave with $p_0 = 1\ \mathrm{N/m^2}$ and spatial dependence α_m will here be denoted by the modal sensitivity function $G_n(x, \alpha_m, \omega)$. The sensitivity function, in turn, is the response to the same pressure at any position $\mathbf{r} = (x, \varphi)$ on the cylinder and is related to the modal sensitivity function by

$$G(\mathbf{r}, \alpha_m, \omega) = G_n(x, \alpha_m, \omega) \cos(n\varphi). \tag{32}$$

This function may, similar to Newland [6, Chapter 16], also be expressed as an integral

$$G(\mathbf{r}, \alpha_m, \omega) = \int_S H(\mathbf{r}, \mathbf{s}, \omega) e^{-i\alpha_m x_s} \cos(n\varphi_s)\, d\mathbf{s}, \tag{33}$$

where $\mathbf{s} = (x_s, \varphi_s)$. S is the surface of the structure and $H(\mathbf{r}, \mathbf{s}, \omega)$ represents the response at location $\mathbf{r}$ to a harmonic point load of unit magnitude at location $\mathbf{s}$. From reasons of symmetry the modal response $W_n(x)$ of the structure to the pressure wave $p_0 e^{-i\alpha_m x} \sin(n\varphi)$ will be the same, except of course that the radial displacement now has a sinusoidal φ dependence. Thus the sensitivity function is in this case given by

$$G(\mathbf{r}, \alpha_m, \omega) = G_n(x, \alpha_m, \omega) \sin(n\varphi). \tag{34}$$

4. Pipe response to TBL excitation

4.1. Response to distributed random excitation

The response to distributed random excitation is given by Newland [6] as

$$S_{WW}(\mathbf{r}_1, \mathbf{r}_2) = \int_S \int_S H^*(\mathbf{r}_1, \mathbf{s}_1, \omega) H(\mathbf{r}_2, \mathbf{s}_2, \omega) S_{PP}(\mathbf{s}_1, \mathbf{s}_2, \omega)\, d\mathbf{s}_1\, d\mathbf{s}_2, \tag{35}$$

where the cross spectral densities of the response and the pressure are defined by

$$\begin{aligned} S_{WW}(\mathbf{r}_1, \mathbf{r}_2, \omega) &= \langle W^*(\mathbf{r}_1, \omega), W(\mathbf{r}_2, \omega) \rangle, \\ S_{PP}(\mathbf{s}_1, \mathbf{s}_2, \omega) &= \langle P^*(\mathbf{s}_1, \omega), P(\mathbf{s}_2, \omega) \rangle. \end{aligned} \tag{36}$$

$\langle\ \rangle$ denotes statistical expectation. If the distributed excitation $P(\mathbf{s}, \omega)$ is assumed to be a sample function from a process, which is stationary and homogenous in space, $S_{PP}(\mathbf{s}_1, \mathbf{s}_2, \omega)$ is a function of only the frequency and the spatial separations,

$$\xi_x = x_{s1} - x_{s2} \quad \text{and} \quad \xi_\varphi = \varphi_{s1} - \varphi_{s2}. \tag{37}$$

This assumption is valid for most large structures excited by a stationary turbulent flow. Far downstream, e.g., $80R$, from pipe singularities such as the entrance or a bend, the boundary layer fills the entire pipe and the flow can be assumed stationary and homogeneous in space, see Ref. [19]. From now on S_{PP} is therefore a function of the spatial separations only.

4.2. Cross-spectral density of the pressure

The pressure cross spectrum is described by Corcos' model [12]. From a curve fit for the narrowband spatial correlation between wall pressures, Corcos obtained

$$S_{PP}(\mathbf{s}_1, \mathbf{s}_2, \omega) = \Phi_{pp}(\omega) \mathrm{e}^{-c_\varphi R\omega|\xi_\varphi|/U_c} \mathrm{e}^{-c_x\omega|\xi_x|/U_c} \mathrm{e}^{\mathrm{i}\omega\xi_x/U_c}, \tag{38}$$

where Φ_{pp} is the wall pressure power spectral density. c_x and c_φ are constants describing the spatial coherence of the wall pressure field, in the longitudinal and circumferential directions, respectively. U_c is the convection velocity. In this work experimentally determined values for Φ_{pp}, c_x, c_φ and U_c are used.

The cross-spectral density of the pressure can be expressed as an exponential Fourier series in the x direction and with a trigonometric Fourier series in the ϕ direction. The period of the exponential Fourier series has to be taken as at least twice the length of the pipe structure, because integral (35) of x_{si} is over the length of the structure and thus ξ_x needs to be evaluated in the interval $-2l_x \ldots 2l_x$. Outside this interval the cross-spectral density can be made periodic as any existing pressure outside the integration limits will not affect the result. Upon this basis the cross-spectral density is given by

$$S_{PP}(\mathbf{s}_1, \mathbf{s}_2, \omega) = \Phi_{pp}(\omega) \sum_{m=-\infty}^{\infty} S_{PPx}(\alpha_m) \mathrm{e}^{\mathrm{i}\alpha_m\xi_x} \sum_{n=1}^{\infty} S_{PP\varphi}(n) \cos(n\xi_\varphi), \tag{39}$$

where

$$\alpha_m = 2\pi m/4l_x. \tag{40}$$

A series expansion with $\sin(n\xi_\varphi)$ does not give any contribution, as the cross-spectral density is symmetric to $\xi_\varphi = 0$. Furthermore the mode $n = 0$ is not included here, as it does not contribute much to the response. The quantities $S_{PPx}(\alpha_m)$ and $S_{PP\varphi}(n)$ are for Corcos' model (38) given by

$$S_{PPx}(\alpha_m) = \frac{1}{4l_x} \int_{-2l_x}^{2l_x} \mathrm{e}^{-c_x\omega|\xi_x|/U_c} \mathrm{e}^{\mathrm{i}\omega\xi_x/U_c} \mathrm{e}^{-\mathrm{i}\alpha_m\xi_x} \,\mathrm{d}\xi_x = \frac{1}{4l_x}\left(\frac{1 - \mathrm{e}^{-d_1 2l_x}}{d_1} + \frac{\mathrm{e}^{d_2 2l_x} - 1}{d_2}\right),$$
$$d_1 = c_x\omega/U_c + \mathrm{i}\omega/U_c - \mathrm{i}\alpha_m, \quad d_2 = -c_x\omega/U_c + \mathrm{i}\omega/U_c - \mathrm{i}\alpha_m, \tag{41}$$

$$S_{PP\varphi}(n) = \frac{2}{2\pi} \int_{-\pi}^{\pi} \mathrm{e}^{-c_\varphi R\omega|\xi_\varphi|/U_c} \cos(n\xi_\varphi) \,\mathrm{d}\xi_\varphi = \frac{1}{\pi}\left(\frac{\mathrm{e}^{d_3\pi} - 1}{d_3} + \frac{\mathrm{e}^{d_4\pi} - 1}{d_4}\right),$$
$$d_3 = -Rc_\varphi\omega/U_c + \mathrm{i}n, \quad d_4 = -Rc_\varphi\omega/U_c - \mathrm{i}n. \tag{42}$$

4.3. Cross-spectral density of the response

The series in Eq. (39) is inserted into integral (35) and the order of summation and integration interchanged

$$\begin{aligned} S_{WW}(\mathbf{r}_1,\mathbf{r}_2,\omega) &= \Phi_{pp}(\omega)\sum_m\sum_n S_{PPx}(\alpha_m)S_{PP\varphi}(n) \\ &\times \int_{-\pi}^{+\pi}\int_{-\pi}^{+\pi}\int_{-l_x}^{+l_x}\int_{-l_x}^{+l_x}(H(\mathbf{r}_1,\mathbf{s}_1,\omega)\mathrm{e}^{-\mathrm{i}\alpha_m x_{s1}})^*(H(\mathbf{r}_2,\mathbf{s}_2,\omega)\mathrm{e}^{-\mathrm{i}\alpha_m x_{s2}}) \\ &\times (\cos(n\varphi_{s1})\cos(n\varphi_{s2})+\sin(n\varphi_{s1})\sin(n\varphi_{s2}))\ R\,\mathrm{d}\varphi_{s1}\ R\,\mathrm{d}\varphi_{s2}\,\mathrm{d}x_{s1}\,\mathrm{d}x_{s2} \\ &= \Phi_{pp}(\omega)\sum_m\sum_n S_{PPx}(\alpha_m)S_{PP\varphi}(n) \\ &\times \{(G_n(x_1,\alpha_m,\omega)\cos(n\varphi_1))^* G_n(x_2,\alpha_m,\omega)\cos(n\varphi_2) \\ &+ (G_n(x_1,\alpha_m,\omega)\sin(n\varphi_1))^* G_n(x_2,\alpha_m,\omega)\sin(n\varphi_2)\}. \end{aligned} \tag{43}$$

The definitions of the sensitivity functions in Eqs. (32)–(34) were used. These functions describe the response to travelling pressure waves and were previously calculated with the spectral FEM in Section 3. Considering only the auto-spectral density of the response at location $\mathbf{r}$ gives specifically

$$S_{WW}(\mathbf{r},\mathbf{r},\omega)=\Phi_{pp}(\omega)\sum_m\sum_n S_{PPx}(\alpha_m)S_{PP\varphi}(n)|G_n(x,\alpha_m,\omega)|^2. \tag{44}$$

Hence the auto-spectral density has no φ dependence, which is expected from reasons of symmetry and the assumption of a homogeneous TBL.

5. Vibrational response of pipe structure

In this section, the theory from Sections 2 and 3 is validated by comparing calculated dispersion characteristics and impulse response functions with both simplified cylinder theory and Arnold–Warburton theory. The developed method in Section 4, in combination with the simplified cylinder theory, is then used to predict the TBL-induced vibration velocity and a comparison with measurements is made.

5.1. Pipe structure

A thin-walled cylindrical pipe was excited by a fully developed internal turbulent flow. The pipe material was steel with density $\rho = 7850\ \mathrm{kg/m^3}$, Young's modulus $E = 215$ GPa and the Poisson ratio $\nu = 0.32$. The damping was modeled with a complex Young's modulus $E(1+\mathrm{i}\eta)$, where the frequency-independent loss factor $\eta = 5\times10^{-4}$ was found from measurements. The geometrical data were as follows: half the length $l_x = 0.23$ m, radius $R = 0.0625$ m and wall-thickness $h = 0.5$ mm. It was presumed that the pipe motion was blocked at the ends, as the test section was fitted to thick-walled cylinders. The investigated frequency range is well below the ring frequency,

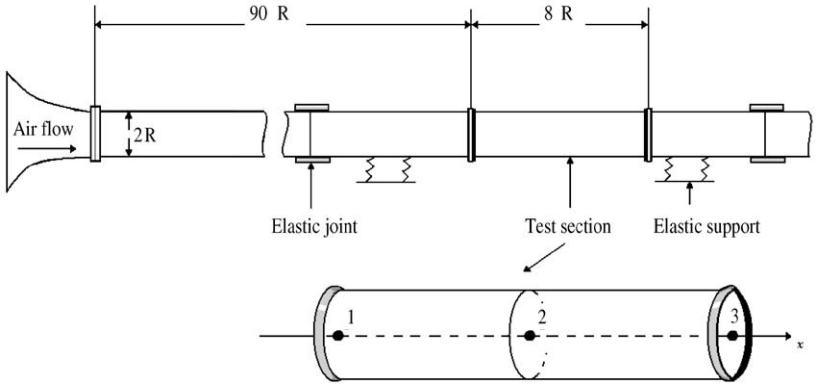

Fig. 2. Pipe rig facility and spectral finite element model of test section with three nodes.

which for this pipe is at approximately 13 kHz. Fig. 2 shows a part of the pipe rig facility and the spectral finite element model of the test section. One spectral finite element fully describes the forced motion to distributed excitation of a free or simply supported pipe. With clamped conditions one more element has to be used as otherwise all nodal degrees of freedom are restrained. The test section was mounted in the wind tunnel of the Acoustics Center of École Centrale de Lyon, 5.5 m downstream from the pipe entrance to achieve a homogeneous and stationary flow in the test section. Acoustic mufflers were located both upstream and downstream of a centrifugal blower, that propelled the air, in order to reduce the background noise. Furthermore, the various pipe sections were accurately matched to avoid disturbances due to any discontinuities. The measurements confirmed a difference of 30 dB between the vibration level of the test section and the rest of the pipe.

5.2. *Wavenumbers*

In Fig. 3 the calculated wavenumbers for propagating waves are compared for the simplified theory and the more accurate Arnold–Warburton theory. The wavenumbers for the simplified theory were calculated in Appendix B. For the Arnold–Warburton theory, the same approach as described by Leissa [13, Chapter 2.2] was used. From the figure it is seen that the results are in good agreement for frequencies up to 3000 Hz, with relative differences below 10%. At frequencies somewhere above 6000 Hz, i.e., half the ring frequency, the use of the simplified cylinder theory becomes questionable for the pipe investigated here.

5.3. *Resonance frequencies*

The pipe resonance frequencies are found from the maxima of $\det(\mathbb{D}^{-1})$. Both the Arnold–Warburton theory and the simplified theory agree well with experimental results. The relative difference between the predicted and measured frequencies are less than 3%, excluding f_{12}, which differs by 6%, see Table 1.

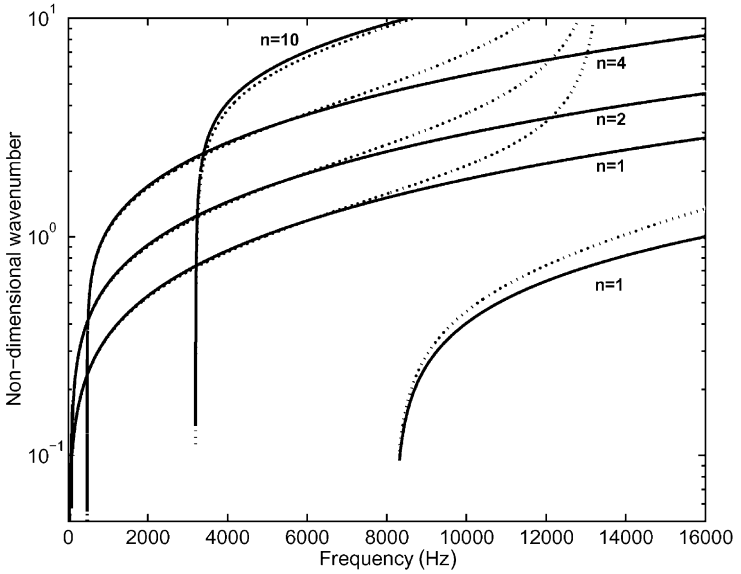

Fig. 3. Wavenumber times radius for various circumferential modes n. Solid, simplified cylinder theory; dotted, Arnold–Warburton theory.

5.4. Response to point force excitation

To develop an understanding for the convergence of the response to distributed excitation, a point force was decomposed into a series of cosine waves in the φ direction and an exponential Fourier series in the x direction:

$$F_0\delta(x-x_s)\delta(\varphi-\varphi_s) \approx F_0\frac{1}{2l_x}\sum_{m=-M}^{M} e^{i2m\pi x/2l_x}e^{-i2m\pi x_s/2l_x}\frac{1}{2\pi}\left(1+2\sum_{n=1}^{N}\cos(n(\varphi-\varphi_s))\right), \tag{45}$$

for large values of M and N. The constant term can be ignored in the expression within parentheses, since it is a constant pressure term and will only excite the breathing mode $n=0$, which has a small mobility well below the ring frequency. To each of these terms the derived spectral FEM in Section 3 can predict the response and the total response is then given by superposition.

A point force was applied in the middle of the clamped pipe and the forced radial displacement at a point located 20 cm from the pipe end was calculated with the spectral FEM. Both the simplified cylinder theory and the Arnold–Warburton theory was used. The simplified theory requires two boundary conditions at each end. Thus for a clamped pipe the displacements U_n and W_n are set to zero. The Arnold–Warburton theory has four boundary conditions and the added conditions at the edges, $V_n=0$ and $\mathrm{d}W_n/\mathrm{d}x=0$, can be satisfied. The calculated results are compared in Fig. 4. The difference between the methods increases with higher frequencies, which

Table 1
Resonance frequencies of in vacuo pipe (Hz)

f_{mn}	m					
	1	2	3	4	5	6
$n=1$	*2091*					
	(2094)					
	—					
$n=2$	*976*	*2217*				
	(982)	(2247)				
	919	—				
$n=3$	*574*	*1295*	*2230*			
	(577)	(1314)	(2273)			
	565	**1301**	—			
$n=4$	*571*	*937*	*1528*	*2250*		
	(572)	(948)	(1560)	(2306)		
	571	**945**	**1560**	—		
$n=5$	*799*	*952*	*1282*	*1757*	*2327*	
	(799)	(960)	(1305)	(1801)	(2397)	
	795	**960**	**1311**	**1815**	—	
$n=6$	*1139*	*1207*	*1371*	*1651*	*2030*	*2485*
	(1138)	(1212)	(1389)	(1687)	(2092)	(2574)
	1131	**1206**	**1387**	**1700**	—	—
$n=7$	*1557*	*1593*	*1679*	*1836*	*2071*	*2377*
	(1554)	(1596)	(1694)	(1868)	(2125)	(2459)
	1544	**1589**	**1689**	**1874**	—	—

Italics: predictions with spectral FEM, simplified theory; (…): predictions with spectral FEM, Arnold–Warburton theory; bold: measurements.

is only expected from the simplifications made in Section 2. In the figure is also shown the forced response to an approximate point force, with $M, N = 5$ in Eq. (45), calculated with the simplified theory. By adding more terms this solution could be seen to converge towards the expected response from a point force. This analysis shows that the developed scheme for distributed excitation is working.

5.5. Turbulence excitation

The pipe was excited by the wall pressure fluctuations induced by an internal turbulent flow and in order to estimate the various parameters in Corcos' model (38). The thin test section was replaced by a rigid section equipped with nine flush-mounted Brüel and Kjær 4135 microphones with an external diameter of 6.35 mm. By comparing the measured r.m.s. value of the displacement of the test section, which was approximately 0.26 μm, with the viscous sub-layer thickness of approximately 12.5 μm, it was a reasonable assumption that the vibrations of the test section did not modify the turbulent wall pressure field. Two measurement series were then made to describe the cross spectrum in the longitudinal and circumferential direction respectively. First, the microphones were located along a line in the longitudinal direction with microphone spacings

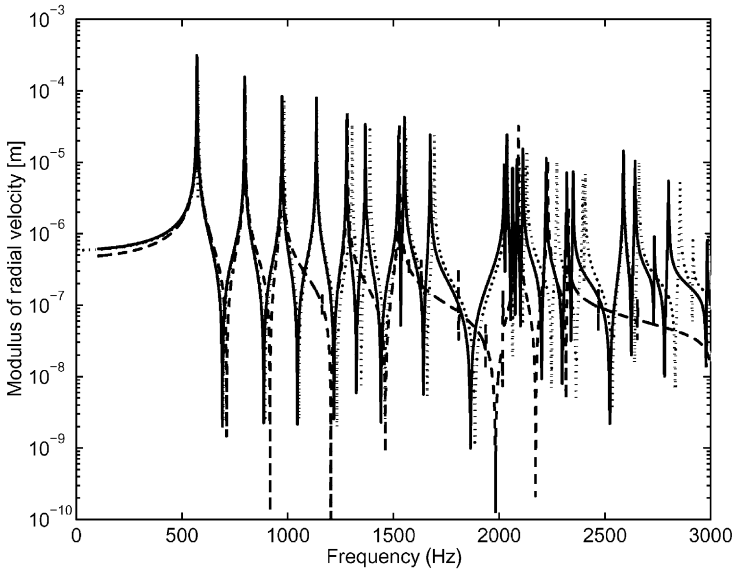

Fig. 4. Transfer mobility. Solid, simplified cylinder theory; dotted, Arnold–Warburton theory; dashed, simplified cylinder theory with approximate point force $M, N = 5$.

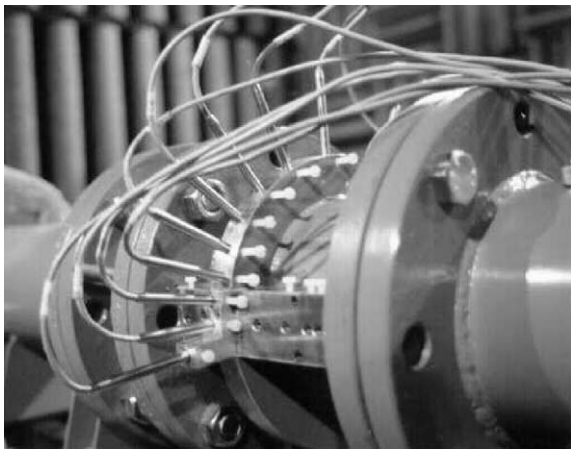

Fig. 5. Circumferential positioning of microphones to measure wall pressure cross spectrum.

varying from 8 to 144 mm. Next, the microphones were located on the circumference with angular separations varying from 8 to 120°. Fig. 5 shows the circumferential configuration.

From rough frequency-independent estimates of the measurement results, the various parameters were found to be [1]: $c_x = 0.15$, $c_\varphi = 0.75$ and $U_c = 0.75U_0$, with U_0 the centre line velocity of 100 m/s. An alternative estimate for c_x and c_φ was given in Ref. [11] with the values of 0.09 and 0.6, respectively. The difference reflects the difficulties in adapting the approximate Corcos model to measurement results. Both sets of parameters are used here to show the

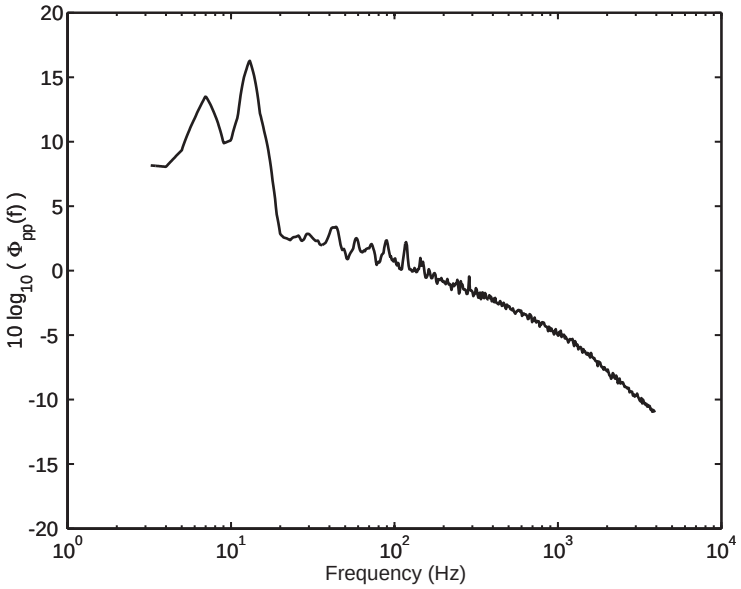

Fig. 6. Wall pressure power spectral density for a centre line velocity of 100 m/s.

sensitivity of the vibration predictions to these parameters. The pressure auto spectrum, $\Phi_{pp}(\omega)$, was taken directly from measurement results, see Fig. 6. In the low-frequency range, below 200 Hz, some peaks occur in Fig. 6. These peaks were identified as longitudinal acoustic modes that occur in the pipe between the ends and can be predicted as in Ref. [20]. In the high-frequency range the decrease of the pressure auto-spectrum is theoretically accentuated by the spatial averaging over the face of the microphone and Corcos [12] therefore proposed a frequency correction. However, given a centre line velocity of 100 m/s and a microphone diameter of 6.35 mm, this correction is negligible in the frequency range of interest here, i.e., 0–3000 Hz.

5.6. *Vibrational response to turbulence excitation*

When predicting the response to turbulence excitation, all the theory derived so far will prove useful. First, the sensitivity function is found with the SFEM in combination with the simplified cylinder theory, and then the response is predicted with Eq. (44). In this equation ten circumferential modes were considered, i.e., $n = 1, \ldots, 10$ and the response converged for $m \geqslant 10$.

Fig. 7 compares the predicted auto-spectrum of the vibration velocity at a point, located 20 cm upstream from the pipe end, to measurement results. The prediction was based on the parameters for Corcos' model given in reference [1], i.e., ($c_x = 0.15$, $c_\varphi = 0.75$). The frequency resolution was 0.05 Hz at 500 Hz and then logarithmically spaced. This was sufficient to capture the amplitudes of all resonances. The figure shows the response integrated to the 1 Hz bandwidth from the measurements. The acceleration measurements were made with both very light Brüel and Kjær 4374 (0.65 g) piezoelectric accelerometers and a laser vibrometer POLYTEC (OFV-302). As the

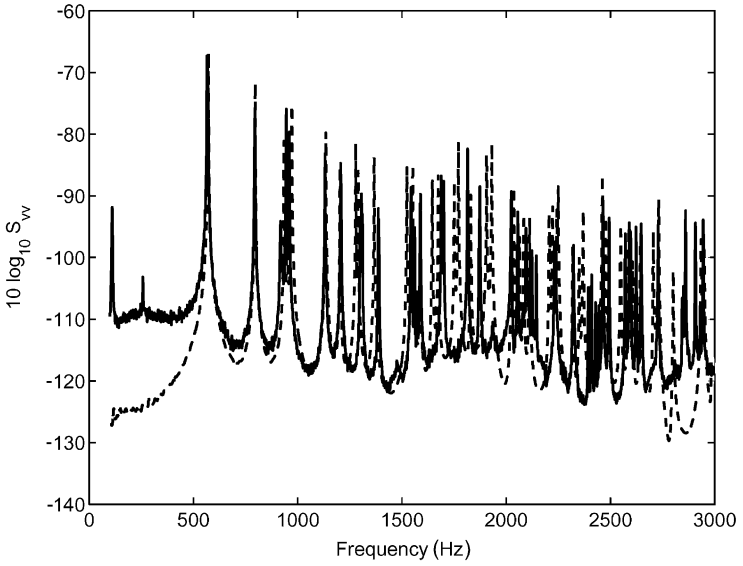

Fig. 7. Vibrational velocity of turbulence excited pipe, dB rel 1 m^2/s^2. Solid line, measured; dashed line, as calculated with Eq. (44).

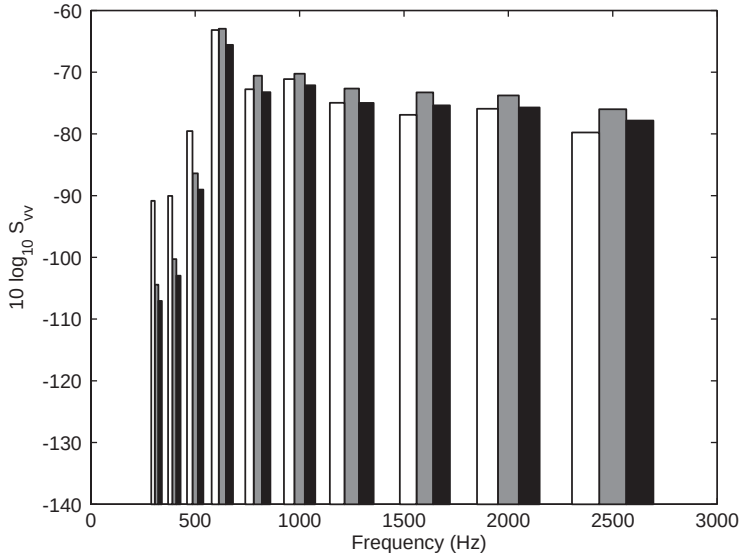

Fig. 8. As in Fig. 7, but in 1/3-octave bands. (□), measured; (▒), calculated with parameters from Ref. [1]; (▓), calculated with parameters from Ref. [11].

surface mass of the test section was as low as 3.9 kg/m^2, the accelerometers introduced a non-negligible added mass effect and therefore only the results from the non-contact laser measurements were used in this paper.

The first resonance was at 565 Hz, see Table 1. Below this frequency the velocity amplitude should decrease with decreasing frequency, since the pipe motion is blocked at the ends. The measurements, however, showed constant amplitudes at low frequencies. Most likely, this was either due to measurement noise or to global vibrations of the entire measurement set up.

Fig. 8 compares measured and calculated results in 1/3-octave bands. The first pipe resonance falls within the 630 Hz band and from this band and upwards in frequency the results show good agreement. The spectral FE model overpredicted the power spectral density of the velocity with about 3 dB if the parameters for Corcos model in Ref. [1] were used. If instead the parameters were taken from Ref. [11], i.e., as ($c_x = 0.09,\ c_\phi = 0.6$), the difference between measured and predicted results in 1/3-octave bands was reduced to less than 2 dB from the 800 Hz band and up, but the difference in the lower bands increased.

Keeping in mind that the damping loss factor is not likely to be constant with frequency and that the use of Corcos' model is known to overpredict the response in the low wavenumber domain [21], these results are encouraging. The use of the simplified cylinder theory and Eq. (44) seem to be applicable and result in moderate calculation times. Six thousand logarithmically spaced frequency points required a computational time of approximately 5 min on a 1 GHz personal computer. Hence, the method seems to be at least 20 times faster than a previous numerical method, based on a boundary integral formulation and a matched asymptotic expansion [1]. It also allows the prediction of the power spectral density of the velocity at any point on the pipe with no extra calculation effort.

6. Conclusions

The aim of this study was to develop an efficient numerical method for the prediction of turbulence-induced vibration in pipe structures. This is achieved by first deriving the sensitivity function, i.e., the structural response to a travelling pressure wave, using a spectral FEM for distributed excitation. The cross-spectral density of the TBL wall pressure is then expressed as a finite Fourier series and the structural response to each term in this series is calculated. The total response to random excitation is given by synthesis of these responses.

The calculations are based on a simplified cylinder theory [15]. A comparison between this and the Arnold–Warburton theory proved the usefulness of the simplified theory in a lower frequency regime. The procedure presented in Sections 2 and 3 may also be applied to all the other thin circular cylindrical shell theories given in Ref. [16, Chapter 2].

The turbulence induced vibration of a pipe was calculated and the results compare favourably with measurement results. The presented approach makes a direct comparison between the spatial characteristics of the random excitation and of the structural response possible [5]. Many different descriptors of the turbulence excitation can be included in the formulation as long as they have a Fourier series expansion in the wavenumber domain. A Chase model [14] has been handled by the authors by employing a fast Fourier transform to evaluate the Fourier series expansion. If the correlation lengths and convection velocity vary as functions of frequency, this can easily be accounted for in Eqs. (41) and (42).

Acknowledgements

This work was supported by the Swedish Research Council (260-2000-444) and the European Commission, ENABLE (GRD4_CT-00-00223).

Appendix A. Calculation of the Lagrangian

Lagrangian (5) is to be evaluated.

$$L = \frac{1}{R}\int_0^{2\pi}\int_{-l_x}^{+l_x}\left\{\frac{Eh}{(1-\nu^2)}(I_{D\text{–}M}(U,V,W,U^a,V^a,W^a)+\beta I_{MOD}(U,V,W,U^a,V^a,W^a)) - \rho h R^2\omega^2(U^aU+V^aV+W^aW)\right\}\mathrm{d}x\,\mathrm{d}\varphi. \tag{A.1}$$

Since the displacement functions are functions of x, the variable substitution $x = Rs$ was made. $I_{D\text{–}M}$ and I_{MOD} are given by Leissa [16, Eqs. (2.11) and (2.12a)]

$$I_{D\text{–}M} = \left(\frac{\partial U^a}{\partial s}+\frac{\partial V^a}{\partial\varphi}+W^a\right)\left(\frac{\partial U}{\partial s}+\frac{\partial V}{\partial\varphi}+W\right) - (1-\nu)\left(\frac{\partial U^a}{\partial s}\left(\frac{\partial V}{\partial\varphi}+W\right)+\frac{\partial U}{\partial s}\left(\frac{\partial V^a}{\partial\varphi}+W^a\right)-\frac{1}{2}\left(\frac{\partial V^a}{\partial s}+\frac{\partial U^a}{\partial\varphi}\right)\left(\frac{\partial V}{\partial s}+\frac{\partial U}{\partial\varphi}\right)\right) + \beta\left\{(\nabla^2W^a)(\nabla^2W)-(1-\nu)\left(\frac{\partial^2W^a}{\partial s^2}\frac{\partial^2W}{\partial\varphi^2}+\frac{\partial^2W}{\partial s^2}\frac{\partial^2W^a}{\partial\varphi^2}-2\left(\frac{\partial^2W^a}{\partial s\partial\varphi}\right)\left(\frac{\partial^2W}{\partial s\partial\varphi}\right)\right)\right\}, \tag{A.2}$$

$$I_{MOD} = -\frac{\partial V^a}{\partial\varphi}\nabla^2W-\frac{\partial V}{\partial\varphi}\nabla^2W^a+\left(\frac{\partial V^a}{\partial\varphi}\right)\left(\frac{\partial V}{\partial\varphi}\right) - (1-\nu)\left(-\frac{\partial V^a}{\partial\varphi}\frac{\partial^2W}{\partial s^2}-\frac{\partial V}{\partial\varphi}\frac{\partial^2W^a}{\partial s^2}+2\frac{\partial V^a}{\partial s}\frac{\partial^2W}{\partial s\partial\varphi}+2\frac{\partial V}{\partial s}\frac{\partial^2W^a}{\partial s\partial\varphi}-2\left(\frac{\partial V^a}{\partial s}\right)\left(\frac{\partial V}{\partial s}\right)\right). \tag{A.3}$$

A.1. Arnold–Warburton theory

The modal displacement functions are defined by Eq. (7). The displacement functions for the adjoint system are given on a similar form:

$$\begin{aligned} U^a(x,\varphi) &= U_n^a(x)\cos(n\varphi),\\ V^a(x,\varphi) &= V_n^a(x)\sin(n\varphi),\\ W^a(x,\varphi) &= W_n^a(x)\cos(n\varphi). \end{aligned} \tag{A.4}$$

Substituting the expressions for the displacements into the Lagrangian and integrating over φ produces the modal Lagrangian L_n,

$$L_n = \frac{\pi}{R}\int_{-l_x}^{+l_x}\left\{\frac{Eh}{(1-\nu^2)}(\boldsymbol{\varepsilon}^a)^{\mathrm{T}}(\mathbf{I}_n+\beta\mathbf{I}_{n\beta})\boldsymbol{\varepsilon} - \rho h R^2\omega^2(U_n^a U_n + V_n^a V_n + W_n^a W_n)\right\}\mathrm{d}x, \tag{A.5}$$

where

$$\boldsymbol{\varepsilon} = (U_n \quad V_n \quad W_n \quad \mathrm{d}U_n/\mathrm{d}x \quad \mathrm{d}V_n/\mathrm{d}x \quad \mathrm{d}W_n/\mathrm{d}x \quad \mathrm{d}^2W_n/\mathrm{d}x^2)^{\mathrm{T}}, \tag{A.6}$$

$\mathbf{I}_n$ and $\mathbf{I}_{n\beta}$ are (7×7) symmetric matrices with non-zero entries given by

$$\begin{aligned}
&(\mathbf{I}_n)_{1,1} = (1-\nu)n^2/2, \quad (\mathbf{I}_n)_{2,2} = n^2, \quad (\mathbf{I}_n)_{3,3} = 1, \quad (\mathbf{I}_n)_{4,4} = R^2,\\
&(\mathbf{I}_n)_{5,5} = (1-\nu)R^2/2, \quad (\mathbf{I}_n)_{1,5} = -(1-\nu)nR/2,\\
&(\mathbf{I}_n)_{2,3} = n, \quad (\mathbf{I}_n)_{2,4} = \nu nR, \quad (\mathbf{I}_n)_{3,4} = \nu R,\\
&(\mathbf{I}_{n\beta})_{2,2} = n^2, \quad (\mathbf{I}_{n\beta})_{3,3} = n^4, \quad (\mathbf{I}_{n\beta})_{5,5} = (1-\nu)2R^2,\\
&(\mathbf{I}_{n\beta})_{6,6} = (1-\nu)2n^2R^2, \quad (\mathbf{I}_{n\beta})_{7,7} = R^4, \quad (\mathbf{I}_{n\beta})_{2,3} = n^3,\\
&(\mathbf{I}_{n\beta})_{3,7} = -n^2\nu R^2, \quad (\mathbf{I}_{n\beta})_{5,6} = (1-\nu)2nR^2,
\end{aligned} \tag{A.7}$$

and $\mathbf{I}_n = \mathbf{I}_n^{\mathrm{T}}$, $\mathbf{I}_{n\beta} = \mathbf{I}_{n\beta}^{\mathrm{T}}$.

A.2. Simplified theory

The modal displacement functions are defined by Eqs. (7) and (9). The displacement functions for the adjoint system are similarly:

$$\begin{aligned}
U^a(x,\varphi) &= U_n^a(x)\cos(n\varphi),\\
V^a(x,\varphi) &= -W_n^a(x)\sin(n\varphi)/n,\\
W^a(x,\varphi) &= W_n^a(x)\cos(n\varphi).
\end{aligned} \tag{A.8}$$

Substituting the expressions for the displacements into the Lagrangian and integrating over φ produces the modal Lagrangian L_n. For reasons mentioned in Section 2, the term proportional to $(\mathrm{d}^2W^a/\mathrm{d}x^2)\mathrm{d}^2W/\mathrm{d}x^2$ is neglected in $\mathbf{I}_{n\beta}^s$. Furthermore $(\mathbf{I}_n^s)_{3,3}$ is changed from R^2 to $R^2(1-\nu^2)$, as suggested in Ref. [15].

$$L_n = \frac{\pi}{R}\int_{-l_x}^{+l_x}\left\{\frac{Eh}{(1-\nu^2)}(\boldsymbol{\varepsilon}^a)^{\mathrm{T}}(\mathbf{I}_n^s+\beta\mathbf{I}_{n\beta}^s)\boldsymbol{\varepsilon} - \rho h R^2\omega^2\left(U_n^a U_n + W_n^a W_n\left(1+\frac{1}{n^2}\right)\right)\right\}\mathrm{d}x, \tag{A.9}$$

where

$$\boldsymbol{\varepsilon} = (U_n \quad W_n \quad \mathrm{d}U_n/\mathrm{d}x \quad \mathrm{d}W_n/\mathrm{d}x)^{\mathrm{T}}, \tag{A.10}$$

$\mathbf{I}_n^s$ and $\mathbf{I}_{n\beta}^s$ are (4×4) symmetric matrices, with non-zero entries given by

$$\begin{aligned}
&(\mathbf{I}_n^s)_{1,1} = (1-v)n^2/2, \quad (\mathbf{I}_n^s)_{3,3} = R^2(1-v^2),\\
&(\mathbf{I}_n^s)_{4,4} = (1-v)R^2/(2n^2), \quad (\mathbf{I}_n^s)_{1,4} = (\mathbf{I}_n^s)_{4,1} = (1-v)R/2,\\
&(\mathbf{I}_{n\beta}^s)_{2,2} = (n^2-1)^2, \quad (\mathbf{I}_{n\beta}^s)_{4,4} = (1-v)2R^2(n^2-1)^2/n^2.
\end{aligned} \tag{A.11}$$

Appendix B. Exact solutions to the equations of motion

The homogeneous equations of motion for the cylindrical shell are given by Eqs. (16) and (17)

$$EI_n \frac{\mathrm{d}^2\theta_n}{\mathrm{d}x^2} - GAK_n\left(\theta_n + \frac{\mathrm{d}W_n}{\mathrm{d}x}\right) + \rho\omega^2 I_n\theta_n = 0,$$

$$GAK_n\left(\frac{\mathrm{d}}{\mathrm{d}x}\left(\theta_n + \frac{\mathrm{d}W_n}{\mathrm{d}x}\right) + N_n\frac{\mathrm{d}^2W}{\mathrm{d}x^2}\right) - (K_w - \omega^2 M_e)W_n = 0.$$

These equations can be expanded to form a set of four first order differential equations. For this purpose the following variable substitution is made:

$$\mathbf{U}_n = (W_n \quad \theta_n \quad \mathrm{d}\theta_n/\mathrm{d}x \quad \gamma_n)^{\mathrm{T}} \quad \text{and} \quad \gamma_n = \theta_n + \frac{\mathrm{d}W_n}{\mathrm{d}x}. \tag{B.1}$$

The variable γ_n is specifically introduced for numerical stability. If instead the more obvious choice $\mathbf{U}_n = (W_n \ \theta_n \ \mathrm{d}\theta_n/\mathrm{d}x \ \mathrm{d}W_n/\mathrm{d}x)^{\mathrm{T}}$ was used, the equations are badly conditioned at low frequencies, where $\theta_n \approx -\mathrm{d}W_n/\mathrm{d}x$. Thus follows

$$\mathrm{d}\mathbf{U}_{n,3}/\mathrm{d}x - (GAK_n/EI_n)\mathbf{U}_{n,4} + (\rho\omega^2 I_n/EI_n)\mathbf{U}_{n,2} = 0, \tag{B.2}$$

$$\mathrm{d}\mathbf{U}_{n,4}/\mathrm{d}x - (N_n/(1+N_n))\mathbf{U}_{n,3} - (K_w - \omega^2 M_e)/(GAK_n(1+N_n))\mathbf{U}_{n,1} = 0, \tag{B.3}$$

or equivalently

$$\frac{\mathrm{d}\mathbf{U}_n}{\mathrm{d}x} = \begin{pmatrix} 0 & -1 & 0 & 1 \\ 0 & 0 & 1 & 0 \\ 0 & \frac{-\rho\omega^2 I_n}{EI_n} & 0 & \frac{GAK_n}{EI_n} \\ \frac{K_w-\omega^2 M_e}{GAK_n(1+N_n)} & 0 & \frac{N_n}{1+N_n} & 0 \end{pmatrix}\mathbf{U}_n. \tag{B.4}$$

Eq. (B.4) can be solved for solutions of the form $\mathrm{e}^{k_{ni}x}$. The four eigenvalues of the matrix on the right-hand side then gives the wavenumbers k_{ni} for a given angular frequency. To each eigenvalue

exists an eigenvector and thus the solutions will be given by

$$\begin{pmatrix} W_n(x) \\ \theta_n(x) \\ \mathrm{d}\theta_n(x)/\mathrm{d}x \\ \gamma_n(x) \end{pmatrix} = \left(\begin{pmatrix} \mathbf{B}_W \\ \mathbf{B}_\theta \\ \mathbf{B}_{\mathrm{d}\theta/\mathrm{d}x} \\ \mathbf{B}_\gamma \end{pmatrix} \mathrm{diag}(\mathrm{e}^{\mathbf{K}x}) \right) \mathbf{C}_n, \tag{B.5}$$

where $\mathbf{B}_{W,\theta,\mathrm{d}\theta/\mathrm{d}x,\gamma}$ are row vectors. $\mathbf{K}$ is a vector with the wavenumbers k_{ni}, 'diag' produces a diagonal matrix from a vector and $\mathbf{C}_n$ is a vector of wave amplitudes.

Appendix C. Evaluation of dynamic stiffness matrix and nodal force vector

With the components of $\mathbf{V}_n$ and $\mathbf{V}_n^a$ from Eqs. (28) and (30), the simplified Lagrangian (13) can be evaluated.

$$\begin{aligned} L_n = \int_{-l_x}^{l_x} \Bigg\{ & B_1 \frac{\mathrm{d}\theta_n^a}{\mathrm{d}x}\frac{\mathrm{d}\theta_n}{\mathrm{d}x} + B_2\left(\theta_n^a + \frac{\mathrm{d}W_n^a}{\mathrm{d}x}\right)\left(\theta_n + \frac{\mathrm{d}W_n}{\mathrm{d}x}\right) + B_3\frac{\mathrm{d}W_n^a}{\mathrm{d}x}\frac{\mathrm{d}W_n}{\mathrm{d}x} \\ & + B_4 W_n^a W_n + B_5\theta_n^a\theta_n - (P_n\mathrm{e}^{-\mathrm{i}\alpha_m x})^* W_n - (P_n\mathrm{e}^{-\mathrm{i}\alpha_m x})W_n^a \Bigg\}\,\mathrm{d}x, \end{aligned} \tag{C.1}$$

where

$$\begin{aligned} & B_1 = EI_n, \quad B_2 = GAK_n, \quad B_3 = GAK_nN_n, \\ & B_4 = (K_w - \omega^2 M_e), \quad B_5 = -\rho\omega^2 I_n. \end{aligned} \tag{C.2}$$

The first variation of this Lagrangian with respect to the nodal displacements $\mathbf{W}_n^a$ is to be zero. The different terms are similar and can be evaluated separately and then added together. Here, the first term in Eq. (C.1) is evaluated to illustrate the procedure:

$$\begin{aligned} & \int_{-l_x}^{l_x} B_1 \frac{\mathrm{d}\theta_n^a}{\mathrm{d}x}\frac{\mathrm{d}\theta_n}{\mathrm{d}x}\,\mathrm{d}x \\ & = B_1 \int_{-l_x}^{l_x} \{((\mathbf{K}.*\mathbf{B}_\theta.*\mathrm{e}^{\mathbf{K}x-\mathbf{K}_p l_x})\mathbf{A}\mathbf{W}_n^a + (\boldsymbol{\alpha}_\mathbf{K}^a.*(\mathbf{B}_\theta \quad c_{n\theta}).*\mathrm{e}^{\boldsymbol{\alpha}_\mathbf{K}^a x-\boldsymbol{\alpha}_{\mathbf{K}_p} l_x})\mathbf{W}_{np}^a)^\mathrm{T} \\ & \qquad \times ((\mathbf{K}.*\mathbf{B}_\theta.*\mathrm{e}^{\mathbf{K}x-\mathbf{K}_p l_x})\mathbf{A}\mathbf{W}_n + (\boldsymbol{\alpha}_\mathbf{K}.*(\mathbf{B}_\theta \quad c_{n\theta}).*\mathrm{e}^{\boldsymbol{\alpha}_\mathbf{K} x-\boldsymbol{\alpha}_{\mathbf{K}_p} l_x})\mathbf{W}_{np})\}\,\mathrm{d}x \\ & = B_1 \int_{-l_x}^{l_x} \{((\mathbf{K}.*\mathbf{B}_\theta.*\mathrm{e}^{\mathbf{K}x-\mathbf{K}_p l_x})\mathbf{A}\mathbf{W}_n^a)^\mathrm{T}((\mathbf{K}.*\mathbf{B}_\theta.*\mathrm{e}^{\mathbf{K}x-\mathbf{K}_p l_x})\mathbf{A}\mathbf{W}_n) \\ & \qquad + ((\mathbf{K}.*\mathbf{B}_\theta.*\mathrm{e}^{\mathbf{K}x-\mathbf{K}_p l_x})\mathbf{A}\mathbf{W}_n^a)^\mathrm{T}(\boldsymbol{\alpha}_\mathbf{K}.*(\mathbf{B}_\theta \quad c_{n\theta}).*\mathrm{e}^{\boldsymbol{\alpha}_\mathbf{K} x-\boldsymbol{\alpha}_{\mathbf{K}_p} l_x})\mathbf{W}_{np}\}\,\mathrm{d}x + O \\ & = \mathbf{W}_n^{a\mathrm{T}}\mathbf{A}^\mathrm{T}B_1((\mathbf{K}.*\mathbf{B}_\theta)^\mathrm{T}(\mathbf{K}.*\mathbf{B}_\theta).*\mathbf{E}_\mathbf{I}(\mathbf{K},\mathbf{K}_p,\mathbf{K},\mathbf{K}_p))\mathbf{A}\mathbf{W}_n \\ & \quad + \mathbf{W}_n^{a\mathrm{T}}\mathbf{A}^\mathrm{T}B_1((\mathbf{K}.*\mathbf{B}_\theta)^\mathrm{T}(\boldsymbol{\alpha}_\mathbf{K}.*(\mathbf{B}_\theta \quad c_{n\theta})).*\mathbf{E}_\mathbf{I}(\mathbf{K},\mathbf{K}_p,\boldsymbol{\alpha}_\mathbf{K},\boldsymbol{\alpha}_{\mathbf{K}p}))\mathbf{W}_{np} + O, \end{aligned} \tag{C.3}$$

where $(.*)$ denotes element wise multiplication (as in MATLAB). O contains terms that do not depend on $\mathbf{W}_n^a$ and therefore do not contribute to the variation. $(\mathbf{v}_1\mathbf{v}_2)^\mathrm{T} = \mathbf{v}_2^\mathrm{T}\mathbf{v}_1^\mathrm{T}$ was used and also that dot products are commutative.

Above the matrix generating function $\mathbf{E_I}$ is defined as

$$\mathbf{E_I}(\mathbf{K}, \mathbf{K_p}, \boldsymbol{\alpha}_\mathbf{K}, \boldsymbol{\alpha}_{\mathbf{K}p}) = \int_{-l_x}^{l_x} (\mathrm{e}^{\mathbf{K}x - \mathbf{K}_p l_x})^{\mathrm{T}} (\mathrm{e}^{\boldsymbol{\alpha}_\mathbf{K} x - \boldsymbol{\alpha}_{\mathbf{K}p} l_x})\, \mathrm{d}x, \tag{C.4}$$

so that its entries are given by

$$\begin{aligned}(\mathbf{E_I})_{ij} = &((\mathrm{e}^{(\mathbf{K})_i(+l_x)-(\mathbf{K}_p)_i l_x})(\mathrm{e}^{(\boldsymbol{\alpha}_\mathbf{K})_j(+l_x)-(\boldsymbol{\alpha}_{\mathbf{K}p})_j l_x}) \\ &- (\mathrm{e}^{(\mathbf{K})_i(-l_x)-(\mathbf{K}_p)_i l_x})(\mathrm{e}^{(\boldsymbol{\alpha}_\mathbf{K})_j(-l_x)-(\boldsymbol{\alpha}_{\mathbf{K}p})_j l_x}))/((\mathbf{K})_i + (\boldsymbol{\alpha}_\mathbf{K})_j).\end{aligned} \tag{C.5}$$

All the terms given in Eq. (C.1) are evaluated in this way and added to get the final expression. The first variation of this new Lagrangian with respect to $\mathbf{W}_n^a$ is to be zero, producing the following system of linear equations in the nodal displacement $\mathbf{W}_n$, the first of which is just Eq. (32),

$$\mathbb{D}_n \mathbf{W}_n = \mathbf{F}_n,$$

$$\mathbb{D}_n = \mathbf{A}^{\mathrm{T}}(\mathbf{Q}_1 .* \mathbf{E_I}(\mathbf{K}, \mathbf{K}_p, \mathbf{K}, \mathbf{K}_p))\mathbf{A}, \tag{C.6}$$

$$\begin{aligned}\mathbf{F}_n = &-\mathbf{A}^{\mathrm{T}}(\mathbf{Q}_2 .* \mathbf{E_I}(\mathbf{K}, \mathbf{K}_p, \boldsymbol{\alpha}_\mathbf{K}, \boldsymbol{\alpha}_{\mathbf{K}p}))\mathbf{W}_{np} \\ &+ \mathbf{A}^{\mathrm{T}} P_n(\mathbf{B}_W^{\mathrm{T}} .* \mathbf{E_I}(\mathbf{K}, \mathbf{K}_p, -\mathrm{i}\alpha_m, 0)),\end{aligned} \tag{C.7}$$

where

$$\begin{aligned}\mathbf{Q}_1 = &B_1(\mathbf{B}_\theta .* \mathbf{K})^{\mathrm{T}}(\mathbf{B}_\theta .* \mathbf{K}) + B_2(\mathbf{B}_\theta + \mathbf{B}_W .* \mathbf{K})^{\mathrm{T}}(\mathbf{B}_\theta + \mathbf{B}_W .* \mathbf{K}) \\ &+ B_3(\mathbf{B}_W .* \mathbf{K})^{\mathrm{T}}(\mathbf{B}_W .* \mathbf{K}) + B_4 \mathbf{B}_W^{\mathrm{T}} \mathbf{B}_W + B_5 \mathbf{B}_\theta^{\mathrm{T}} \mathbf{B}_\theta,\end{aligned}$$

$$\begin{aligned}\mathbf{Q}_2 = &B_1(\mathbf{B}_\theta .* \mathbf{K})^{\mathrm{T}}((\mathbf{B}_\theta \quad c_{n\theta}) .* \boldsymbol{\alpha}_\mathbf{K}) \\ &+ B_2(\mathbf{B}_\theta + \mathbf{B}_W .* \mathbf{K})^{\mathrm{T}}((\mathbf{B}_\theta \quad c_{n\theta}) + (\mathbf{B}_W \quad c_{nW}) .* \boldsymbol{\alpha}_\mathbf{K}) \\ &+ B_3(\mathbf{B}_W .* \mathbf{K})^{\mathrm{T}}((\mathbf{B}_W \quad c_{nW}) .* \boldsymbol{\alpha}_\mathbf{K}) + B_4 \mathbf{B}_W^{\mathrm{T}}(\mathbf{B}_W \quad c_{nW}) + B_5 \mathbf{B}_\theta^{\mathrm{T}}(\mathbf{B}_\theta \quad c_{n\theta}).\end{aligned} \tag{C.8}$$

References

[1] C. Durant, G. Robert, P.J.T. Filippi, P.O. Mattei, Vibroacoustic response of a thin cylindrical shell excited by a turbulent internal flow: comparison between numerical prediction and experimentation, *Journal of Sound and Vibration* 229 (2000) 1115–1155.

[2] J. Horáček, The computation of the dynamic response of cylindrical shells in a turbulent flow, *Acta Technica ČSAV* 117 (2) (1986) 214–229.

[3] S. Finnveden, Exact spectral finite element analysis of stationary vibrations in a railway car structure, *Acta Acustica* 117 (2) (1994) 461–482.

[4] S. Finnveden, Spectral finite element analysis of the vibration of straight fluid-filled pipes with flanges, *Journal of Sound and Vibration* 199 (1997) 125–154.

[5] F. Birgersson, N.S. Ferguson, S. Finnveden, Application of the spectral finite element method to turbulent boundary layer induced vibration of plates, *Journal of Sound and Vibration* 259 (2003) 873–891.

[6] D.E. Newland, *An Introduction to Random Vibration and Spectral Analysis*, Longman, New York, 1984.

[7] Y.K. Lin, *Probabilistic Theory of Structural Dynamics*, McGraw-Hill, New York, 1967.

[8] C. Maury, P. Gardonio, S.J. Elliott, A wavenumber approach to modelling the response of a randomly excited panel, Part i: general theory, *Journal of Sound and Vibration* 252 (2002) 83–113.

[9] R.S. Langley, Application of the dynamic stiffness method to the free and forced vibration of aircraft panels, *Journal of Sound and Vibration* 135 (1989) 319–331.
[10] F. Birgersson, Modelling with the Dynamic Stiffness and the Spectral Finite Element Methods for Distributed Sources, M.Sc. Thesis, ISVR, The University of Southampton, 2000.
[11] C. Durant, Etude Expérimentale de l'Excitation et de la Réponse Vibroacoustique d'une Conduite Sollicitée par un Écoulement Interne, Ph.D. Thesis, Laboratoire de Méchanique des Fluides et d'Acoustique, École Centrale de Lyon, 1999.
[12] G.M. Corcos, The resolution of turbulent pressure at the wall of a boundary layer, *Journal of Sound and Vibration* 6 (1967) 59–70.
[13] J.E. Ffowcs Williams, Boundary-layer pressures and the corcos model: a development to incorporate low-wavenumber constraints, *Journal of Fluid Mechanics* 125 (1982) 9–25.
[14] D.M. Chase, Modelling the wavevector-frequency spectrum of turbulent boundary layer wall-pressure, *Journal of Sound and Vibration* 70 (1980) 29–67.
[15] S. Finnveden, Simplified equations of motion for the radial–axial vibrations of fluid filled pipes, *Journal of Sound and Vibration* 208 (1997) 685–703.
[16] A.W. Leissa, *Vibration of Shells*, Acoustical Society of America; Originally issued by NASA 1973 SPP 288, 1993.
[17] P.M. Morse, H. Feshbach, *Methods of Theoretical Physics*, McGraw-Hill, New York, 1953.
[18] J.F. Doyle, *Wave Propagation in Structures*, Springer, New York, 1997.
[19] J. Sabot, G. Comte-Bellot, Intermittency of coherent structures in the core region of fully developed turbulent pipe flow, *Journal of Fluid Mechanics* 74 (4) (1976) 767–796.
[20] V. Mason, Some experiments on the propagation of sound along a cylindrical duct containing flowing air, *Journal of Sound and Vibration* 10 (1969) 208–226.
[21] N.C. Martin, P. Leehey, Low wave number wall pressure measurements using a rectangular membrane as a spatial filter, *Journal of Sound and Vibration* 52 (1977) 95–120.